ACS Sustainable Chemistry & Engineering

pubs.acs.org/journal/ascecg

Research Article

Insight into the Synthetic Mechanism of Cadmium-Free Blue-Emissive Quantum Dots for Eco Light-Converting System

Ho Kyung Lee, Ji Hyeon Kim, Il Tae Kim, Dal Ho Lee, and Chan Ho Park*

Cite This: *ACS Sustainable Chem. Eng.* 2024, 12, 2588−2597

Read Online

ACCESS | Metrics & More | Article Recommendations | Supporting Information

ABSTRACT: Cd-free nanocrystals, such as $CuCrS_2$/ZnS (CCS/ZnS) quantum dots (QDs), have been highlighted as potential blue-emitting probes. However, the relatively irregular and less uniform morphological structure of QDs synthesized by conventional methods indicated low optical performance with a photoluminescence quantum yield (PLQY) of ∼0.05. Herein, we modified the synthetic method for CCS/ZnS QDs based on the hard and soft acids and bases (HSAB) theory. By using the HSAB-based precursors and appropriate ligand moieties, we synthesized QDs with a uniform morphology and enhanced PLQY of ∼0.16. The core−shell formation of the CCS/ZnS QDs was confirmed using X-ray spectroscopic methods. Consequently, a QD-incorporated polymer matrix as a color filter for a white-light-emitting diode (LED) by hybridizing Cd-free blue-emitting CCS/ZnS QDs and yellow-emitting $CuInS_2$/ZnS/ZnS QDs in poly(methyl methacrylate) was fabricated. Their optical properties were systematically controlled by modifying the ratio of the two QDs, resulting in (CIE_x, CIE_y = 0.254−0.34, 0.245−0.299) of color coordinates and 21914.48 to 5071.39 K of correlated color temperature. This study demonstrates the potential of the environmentally friendly QD-based display technology.

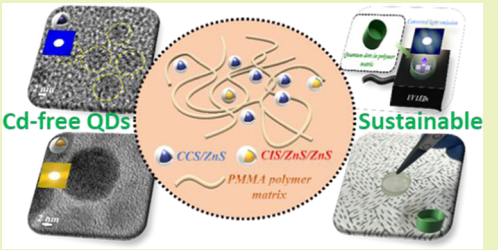

KEYWORDS: *$CuCrS_2$, quantum dots, nanocrystals, blue emission, white-light-converting film, cadmium-free*

Downloaded via GACHON UNIV on February 20, 2024 at 01:14:06 (UTC).
See https://pubs.acs.org/sharingguidelines for options on how to legitimately share published articles.

INTRODUCTION

Colloidal semiconductor nanocrystals, known as quantum dots (QDs), have been considered a tremendously interesting class of materials for the past three decades owing to their unique physical and chemical properties.[1,2] Among these, the cadmium (Cd)-based QDs are the most studied materials because of their full-color tunability over the entire visible region, high photoluminescence quantum yield (PLQY), and photostability.[3] However, Cd-containing products pose challenges during manufacturing and disposal, as environmental regulations restrict their usage due to the inherent toxicity in Cd.[4] Therefore, in order to circumvent environmental regulations and utilize QDs in diverse applications, it is imperative to develop a substitute for Cd.

To ensure the utilization and integration of QDs in the fields of optoelectronics, biology, and biomedicine, it is vital to consider the environmental-friendly attributes of QDs as well as its top-notch performance, including elevated quantum efficiency (QE) and robust environmental stability.[5] In this regard, $CuInS_2$ (CIS), a typical copper-based ternary composite, has attracted attention because its PLQY can be increased to as high as ∼0.8 with a ZnS shell overcoating onto its surface. The emission color of CIS QDs can be tuned from green to the near-infrared (NIR) spectral region by simply controlling the Cu/In molar ratio and size with lower toxicity than Cd-based QDs.[6−8] However, the absence of blue-region emission, which requires a much larger band gap, in CIS QDs has prompted further efforts to find blue-emissive probes suitable for optoelectronic applications. Meanwhile, as the Cd-free QD-based light-emitting diode (LED) systems[9−11] have been developed in these research fields, white-light-emitting diodes (LEDs) are considered a next-generation light source. They are fabricated by combining blue LEDs with fluorescent materials such as fluorophores, and QDs.[12−14] When green and red fluorescent materials were incorporated into blue LED chips, a white LED with a high color rendering index (CRI, R_a) was fabricated. However, multicomponent luminescent layers in LED systems might result in low luminescence efficiency owing to the reabsorption of the emission color.[15,16]

Thus, $CuCrS_2$ has excellent potential as an alternative blue-emitting source exhibiting p-type semiconducting properties with an optical band gap of ∼2.48 eV. $CuCrS_2$ consists of a Cu-based ternary system with a less toxic composition than Cd- and Pb-based QDs.[17] According to the US Agency for Toxic Substances and Disease Registry (ATSDR) 2022 substance priority list, Cd and Pb rank second and seventh, respectively, whereas they rank 17th for Cr^{6+}, 78th for Cr, and 120th for Cu on the list. Thus, $CuCrS_2$ is a rational replacement for conventional QDs, overcoming environmental

Received: September 26, 2023
Revised: December 22, 2023
Accepted: January 4, 2024
Published: January 18, 2024

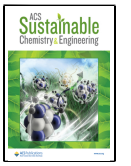

© 2024 American Chemical Society

https://doi.org/10.1021/acssuschemeng.3c06115
ACS Sustainable Chem. Eng. 2024, 12, 2588−2597

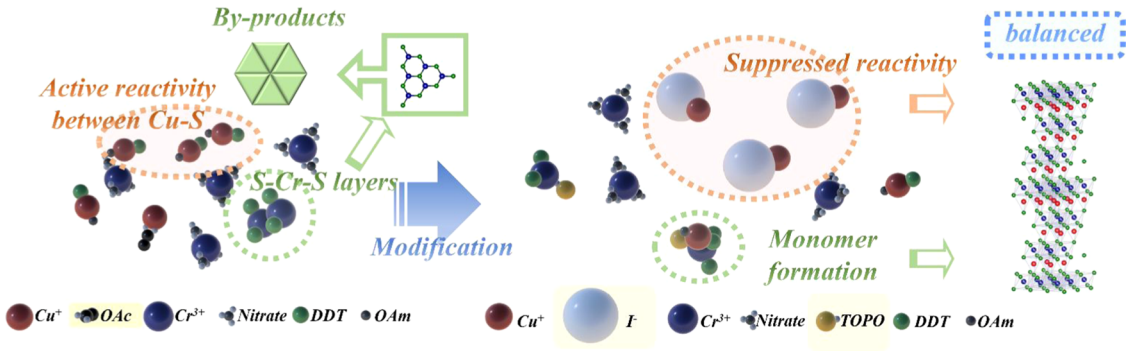

Figure 1. Schematic illustration of true blue-emissive $CuCrS_2$/ZnS QDs synthesis via HSAB-based modification.

and safety issues. However, they have rarely been studied at the nanoscale or as a type of QD with fluorescence (Table S1). Park et al. previously reported blue-emitting $CuCrS_2$/ZnS (CCS/ZnS) QDs via a simple heating-up method with 1-dodecanethiol (DDT) as the surface passivation ligand and sulfur source, which indicated broad blue-cyan fluorescence.[18] Nevertheless, the morphological structure was less uniform with a broad size distribution and the PLQY was limited, restricting further applications. These features indicate the need to improve the synthesis method of CCS/ZnS QDs to be utilized in various applications, including optoelectronics.

Here, we introduce a modified synthesis procedure for CCS/ZnS QDs using hard and soft acids and bases (HSAB). Previous results implied that unbalanced reactivities between two different metal precursors toward the thiol group in DDT, led to a less uniform morphological structure and, eventually, a low optical performance. To solve this problem, we controlled the reactivity of Cu^+ ions because the Cu−S binding affinity is much stronger than that of the Cr^{3+} ion, and employed a co-ligand system with the incorporation of trioctylphosphine oxide (TOPO) as another chelating ligand for Cr^{3+} ions to suppress the Cr_2S_3 side product (Figure 1). The CCS/ZnS QDs synthesized using the modified method exhibited an improved isotropic morphology, narrow size distribution, and emission in the blue spectral region (~430 nm). In addition, for white-light-emitting device applications, the modified CCS/ZnS QDs were mixed with CIS/ZnS/ZnS QDs in a PMMA polymeric matrix. Moreover, Cu-based ternary composites exhibited a large Stokes shift,[19] which reduces multicomponent's spectral overlaps and reabsorption, resulting in an efficient LED or light-converting-system. Furthermore, the dual-component system for light-converting applications provides efficient controllability of the white-light properties by a simple ratio modification of the two QDs. The fabricated film exhibited a bright white-light emission under 365 nm light irradiation. The color coordinates and correlated color temperature (CCT) of the white light from the film were controlled and displayed a broad range of white-light temperatures.

EXPERIMENTAL SECTION

Materials. Copper(I) iodide (CuI, 99.999% trace-metal basis), chromium(III) nitrate nonahydrate ($Cr(NO_3)_3{\cdot}9H_2O$, 99%), copper-(I) acetate (Cu(OAc), 97%), indium acetate ($In(OAc)_3$, 99.99%), zinc(II) acetate dihydrate ($Zn(OAc)_2{\cdot}2H_2O$, 99%), trioctylphosphine oxide (TOPO, 90%), oleylamine (OAm, technical grade, 70%), 1-dodecanethiol (DDT, 98%), octadecene (ODE, technical grade, 90%), poly(methyl methacrylate) (PMMA, containing ~5.0% toluene), and chloroform anhydrous (99%) were purchased from Sigma-Aldrich. Toluene (99%), acetone (99%), and ethyl acetate (99%) were purchased from Daejung Chemicals and Metals. Tetrabutylammonium hexafluorophosphate ($TBAPF_6$, > 98%) was purchased from Tokyo Chemical Industry Corporation, and all of the chemicals were used without further purification.

Characterization. A high-resolution X-ray photoelectron spectroscope (HR-XPS, Nexa, Thermo Fisher Scientific) and a high-resolution X-ray diffractometer (HR-XRD, Smartlab, Rigaku) with Al Kα X-ray and 3 kW Cu X-ray sources were employed for identification of the chemical oxidation and binding states and crystal structure of synthesized QDs, respectively. High-resolution transmission electron microscope (HR-TEM, Tecnai, FEI) was employed to characterize the morphology of the QDs at an accelerating voltage of 300 kV and a resolution of 1.4 Å, and an inductively coupled plasma-optical emission spectrometer (ICP-OES, AVIO550, PerkinElmer) was used to assess the metal ratio of QDs. Ultraviolet/visible/NIR (UV/vis/NIR) spectrophotometry (UV−vis, V-770, Jasco) and a spectrofluorometer (PL, Nanolog, Horiba) were used to characterize the optical properties of the QDs. In addition, to identify the fluorescence lifetime decay, a time-resolved photoluminescence spectroscope (TRPL, Easylife, and PTI) was employed.

Cyclic Voltammetry Analysis for LUMO−HOMO Gap Characterization. To confirm the lowest unoccupied molecular orbital (LUMO) and highest occupied molecular orbital (HOMO) band structures of QDs, cyclic voltammetry (CV) analysis was conducted with a potentiostat (WIZEIS-1200 premium, WizMAC, Inc.). The analysis was performed in 0.1 M $TBAPF_6$ electrolyte (in acetonitrile) with a three-electrode system, Ag/AgCl electrode, and Pt coil electrode, as reference and counter electrodes, respectively. The working electrode was fabricated by simply drop-casting the QD solution onto glassy carbon electrode (GCE). The scan rate was fixed to 50 mV/s. The measured redox potentials were calibrated with reference to the Fe^+/Fc couple.

Synthesis of $CuCrS_2$/ZnS QDs. To synthesize the $CuCrS_2$ core, our previous method was employed with some modifications. Briefly, 20 mL of ODE was placed in a three-neck round-bottom flask. Further, 0.5 mmol of CuI, 0.5 mmol of $Cr(NO_3)_3{\cdot}9H_2O$, 1 mmol of TOPO, and 2.5 mL of OAm were added, and the flask was degassed at 120 °C for 10 min. After 10 min, DDT (5 mL) was injected and degassed for another 10 min. The degassed mixture was then heated to 225 °C and kept for 90 min for monomer formation, nucleation, and crystal growth of the $CuCrS_2$ core. After the core synthesis, the mixture was quenched to ~25 °C to stop the reaction. It is worth noting that during core preparation, several impurities were also synthesized owing to the still unbalanced reactivities of the metal cations or other factors. Therefore, before the simultaneous ZnS shelling process, a one-time centrifugation with a small amount of nonpolar solvent, for example, toluene and chloroform, was better for the preparation of high-quality core/shell structures. After removing impurities, 4 mmol of $Zn(OAc)_2{\cdot}2H_2O$ and OAm (5 mL) were added into the above core solution, and it was degassed at 120 °C for 30 min to remove water molecules and additional nonpolar solvents. After degassing, 1.5 mL of DDT was injected into the mixture followed by heating up to 230 °C and it was kept for 30 min to overcoat the ZnS

https://doi.org/10.1021/acssuschemeng.3c06115
ACS Sustainable Chem. Eng. 2024, 12, 2588−2597

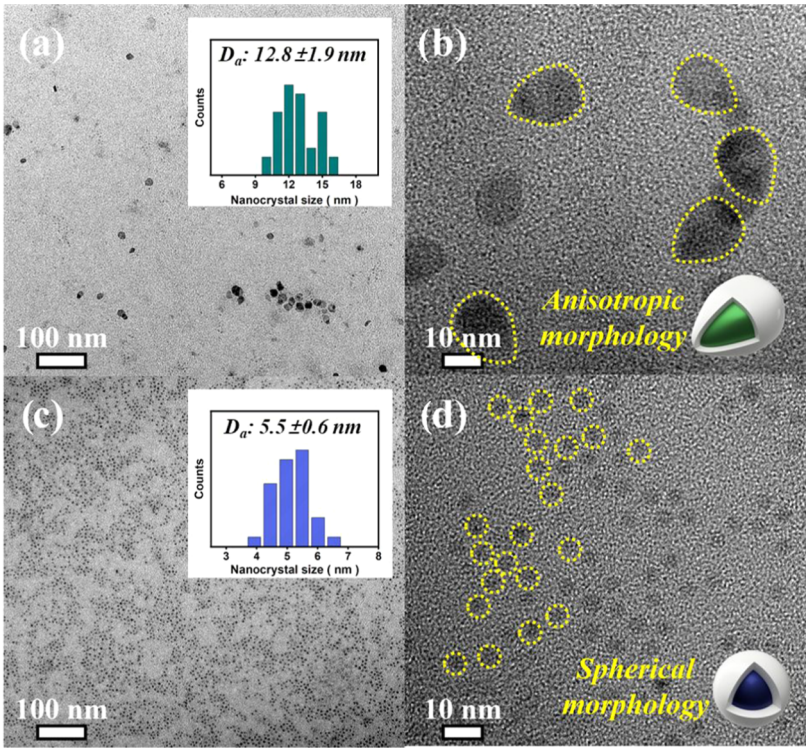

Figure 2. TEM analysis of $CuCrS_2$/ZnS QDs synthesized by (a, b) previously reported method and (c, d) present modified method, respectively, and their corresponding size distribution analysis results (interpolation).

shell onto the CCS core. After the preparation of the core/shell structure, the resulting QDs were isolated by introducing an excess volume of acetone followed by centrifugation. The isolated QDs were purified using a precipitation/redispersion protocol similar to our previous method. Briefly, the isolated QDs were redispersed in a small amount of toluene and precipitated by adding excess ethyl acetate and centrifuging. This step was repeated 3 times to remove the unreacted ligands and residual solvent. Finally, the QDs were dried in a 60 °C vacuum oven for over 24 h and ground for powder sample preparation.

Synthesis of $CuInS_2$/ZnS/ZnS QDs. Bright-yellow light-emitting CIS/ZnS/ZnS core/shell/shell QDs were prepared by using a simple heating method. The synthesis method was similar to that of our CCS QDs preparation method. In a three-neck round-bottom flask, 20 mL of ODE, 0.125 mmol of Cu(OAc), 0.5 mmol of $In(OAc)_3$, and 5 mL of OAm were added, and the reaction flask was degassed at 120 °C for 10 min. After that, DDT (5 mL) was injected into the above mixture, and it was heated up to 225 °C and kept for 90 min to synthesize the CIS core. After the core preparation, the reaction was quenched by cooling the flask down to room temperature to stop the reaction. Then, 4 mmol of $Zn(OAc)_2{\cdot}2H_2O$ and 5 mL of OAm were introduced into the CIS core solution, and they were degassed at 120 °C for 10 min. After that, DDT (1.5 mL) was introduced into the flask, followed by heating up to 230 °C and maintained for 30 min to passivate the CIS core surface by the first ZnS shell. After the first ZnS shelling process, the second ZnS shell was coated onto the CIS/ZnS core/shell using the same procedure as that used for the first shelling process. The synthesized CIS/ZnS/ZnS QDs were isolated by using excess acetone and centrifuged. For the purification step, the precipitation/redispersion method was employed to prepare the CIS/ZnS/ZnS QDs. Briefly, the isolated QDs were redispersed in a small amount of toluene and precipitated by the addition of excess ethyl acetate and centrifuging. This step was repeated 3 times to remove unreacted ligands and excess solvent. Finally, the QDs were dried in a 60 °C vacuum oven for over 24 h and ground for the preparation of powder sample.

Fabrication and Characterization of White-Light-Converting Film. The white-light-converting film was fabricated by using simple mixing, casting, and drying processes. Briefly, the two QDs were mixed in 5 mL of chloroform at various weight ratios (CCS/CIS QDs: 10.0, 20.0, and 40.0). After mixing, the PMMA was dissolved in the QDs solution at a concentration of 5 wt %. The prepared stock solution was cast onto a home-built Teflon-lined vessel (volume capacity of 1 cm^3 in the case of water), and this was dried onto the 50 °C preheated hot plate for over 6 h.

RESULTS AND DISCUSSION

Synthesis of $CuCrS_2$/ZnS QDs. In our previous work, we synthesized CCS/ZnS QDs using Cu(I) acetate and Cr(III) nitrate precursors in a high-boiling solvent, along with the coordinating ligand, OAm, and co-ligand DDT as the sulfur source. However, the synthesized QDs exhibited poor uniformity and quality owing to the unbalanced reactivity of metal cations toward sulfur precursor (thiol), resulting in a side product, Cr_2S_3 nanoflake.[18] Based on these results, it is rational that pairs of precursors and ligands in the synthetic system should be modified to balance their reactivity. According to the hard and soft acids and bases (HSAB) theory, Cu^+ is a typical soft metal (acid), and thiol is a typical soft base, resulting in preferable reactivity. However, Cr^{3+} ($\eta \sim 9.1$ eV) is relatively harder than Cu^+ ($\eta \sim 6.28$ eV),[20−22] causing poor reactivity with thiol functional group. Considering this, we assumed that the reactivity of Cu^+ precursor toward thiol moiety has to be suppressed. In contrast to Cu^+, Cr^{3+} should exist in a more reactive state, but not excessively because the over-relaxed state might cause a side product, for example, Cr_2S_3. Iodide ion, I^-, is a soft base anion,[23,24] and CuI precursor may provide the suppressed reactivity of Cu^+ precursor. Conversely, because Cr^{3+} is a hard acid, the bond nature with thiol functional groups may be more challenging than that of Cu^+, resulting in naturally slow reaction kinetics. Because TOPO is a highly polar molecule owing to the dipolar P═O bond[25] and this

https://doi.org/10.1021/acssuschemeng.3c06115
ACS Sustainable Chem. Eng. 2024, 12, 2588−2597

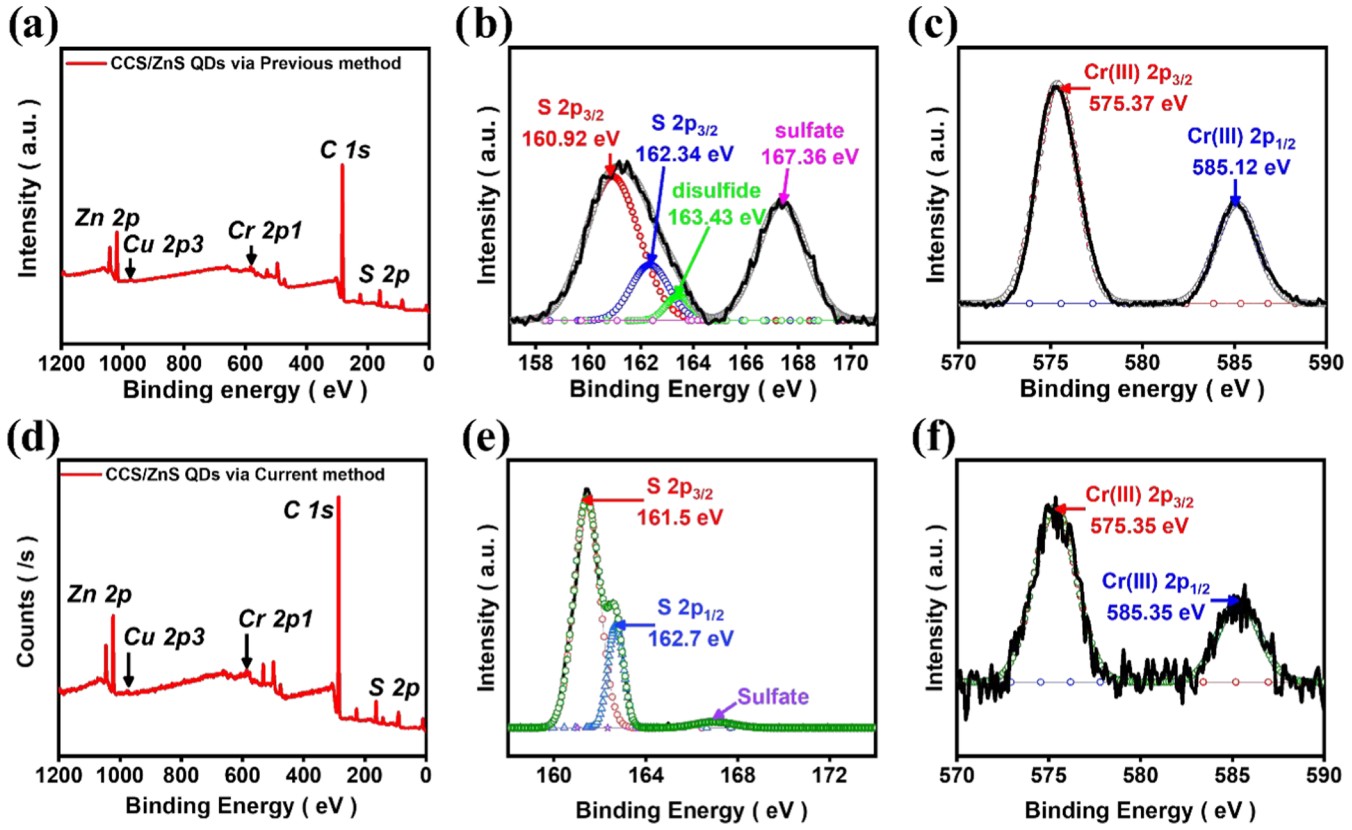

Figure 3. XPS analysis results of $CuCrS_2$/ZnS QDs. (a) $CuCrS_2$/ZnS QDs entire survey; (b) S 2p spectra and (c) Cr 2p spectra of $CuCrS_2$ core prepared by previous method; (d) entire survey of $CuCrS_2$/ZnS QDs; and (e) S 2p spectra and (f) Cr 2p spectra from $CuCrS_2$ core synthesized in the current method, respectively.

high-polarity feature of TOPO may offer a more stable coordination bond with Cr^{3+}, resulting in more suppressed Cr_2S_3 formation owing to the steric hindrance effect. Potentially, this controlled system might offer a more controlled $CuCrS_2$ NCs formation condition, reducing the possibility of side product formation.

The TEM analysis of the CCS/ZnS QDs in this study showed that the QDs had an improved morphological structure with a spherical shape and a more uniform size distribution than those in our previous work (Figure 2). In our previous work, CCS/ZnS QDs prepared by a previously reported method showed an irregular morphology and broad size distribution with an average diameter of 12.8 ± 1.9 nm (Figure 2a,2b). However, our proposed synthetic modification for the preparation of high-quality CCS/ZnS QDs exhibited a more uniform morphology and narrower size distribution, with an average size of 5.5 ± 0.6 nm (Figure 2c,2d). This result indicates that our controlled system can offer more precise QD synthesis with inhibited side-product formation. An XRD analysis was conducted to determine the crystalline structures of the prepared CCS/ZnS QDs. The XRD peaks of the CCS core appeared at 35.48, 38.11, 49.45, and 52.68°, corresponding to the (104), (015), (018), and (110) phases, respectively (Figure S1a). After the ZnS shell overcoated the CCS core NCs, the (101), (012), (104), (018), and (110) peaks appeared at 29.53, 30.86, 34.88, 49.13, and 52.24°, respectively (Figure S1b). The absence of the (101) and (012) phases at 30.01 and 31.16° might be a result of the partial release of Cr^{3+} during the isolation and purification steps. TOPO is a well-known metal extraction agent, and because of this property, some Cr^{3+} atoms might be extracted after washing.[26,27] Nevertheless, as shown in Figure S1b, we could not find any significant difference between the crystal system of CCS/ZnS QDs synthesized by the previously reported and current modified methods, with little amorphous phase, which is probably attributed to the incorporation of DDT into the system. It is worth noting that all peaks are not significantly but slightly shifted toward smaller 2θ value compared with bulk $CuCrS_2$ XRD pattern (Card No.:01−079−7419). This phenomenon may be explained by the lattice parameter difference between $CuCrS_2$ (α = 3.483 Å) and ZnS (α = 5.345 Å), resulting in XRD peak shift toward smaller 2θ,[28] a similar result obtained from our previous work (Figure S1b). Furthermore, to assess an exact metal cation ratio, elemental analysis was investigated by using ICP-OES and XPS (Table S2). The Cu:Cr ratio was confirmed to be 1:3.97 in ICP-OES and 1:1.02 in XPS analysis, respectively, rather different from the ratio that we fed in the reactor. This might be explained by the Zn^{2+} ion etching of the $CuCrS_2$ core with the ejection of Cu ions. Also, the molar ratio of Zn was much higher than the initial feed ratio because the Zn precursor was added after the purification step once the $CuCrS_2$ core had formed. Thus, the actual amounts of Cu and Cr would be much lower than the initial feed amounts. As a result, the Cu/Cr/Zn ratio was 1:1:21 in XPS analysis. In the ICP-OES analysis, the Cr/Zn ratio was 1:22.7, similar to XPS's, although Zn is 90 times higher than Cu. The result of the elemental ratio determined by ICP-OES might have underestimated the Cu element in QDs due to undesired reactions.

https://doi.org/10.1021/acssuschemeng.3c06115
ACS Sustainable Chem. Eng. 2024, 12, 2588−2597

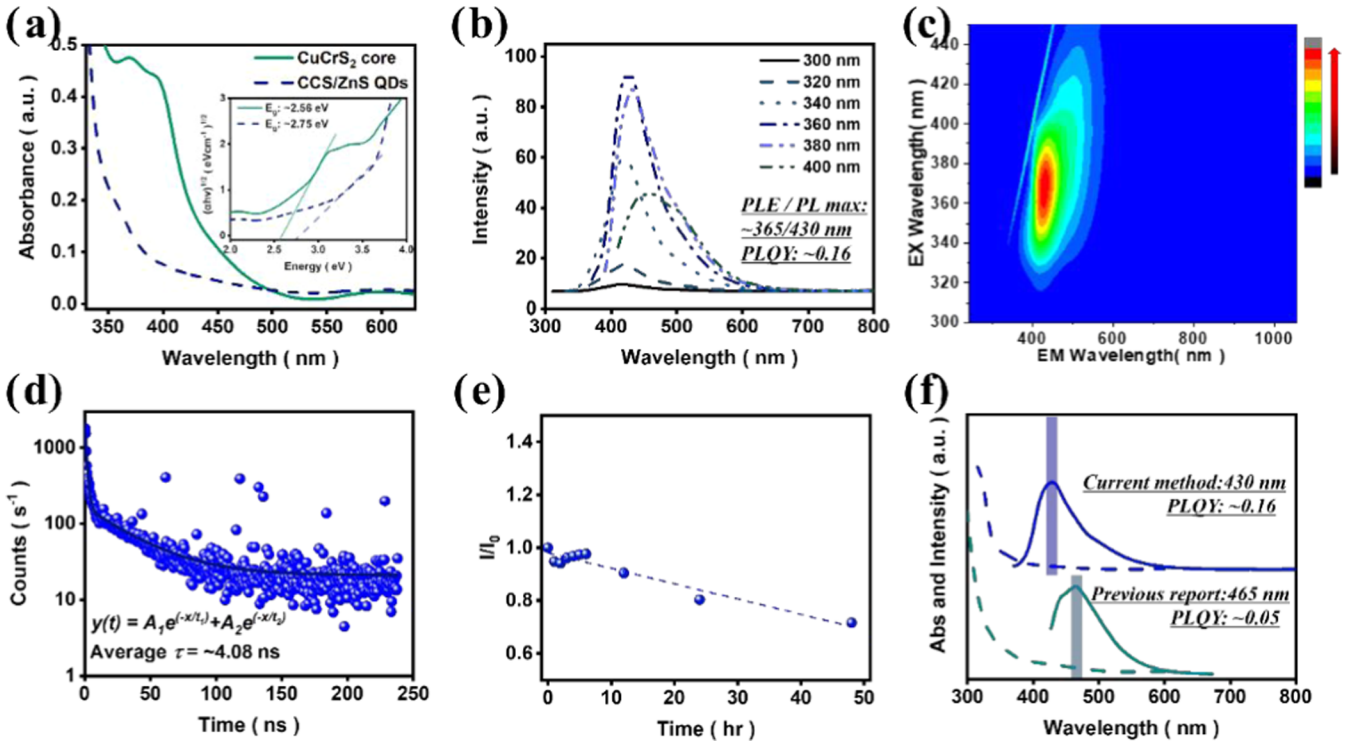

Figure 4. Optical property analysis results of $CuCrS_2$ QDs synthesized by the current method. (a) UV−vis absorption spectra comparison between $CuCrS_2$ core and $CuCrS_2$/ZnS QDs, with Tauc plot calculation comparison (interpolation); (b) PL spectra of $CuCrS_2$/ZnS QDs with various excitation wavelength; (c) corresponding PL mapping result; (d) PL lifetime decay analysis with biexponential decay function fitted result; (e) photostability analysis result under 365 nm UV irradiation; and (f) UV−vis and PL properties comparison between the previous report and current method.

To confirm the chemical oxidation states and binding features of the CCS/ZnS QDs synthesized in this study, XPS analysis was conducted, and the results were compared with those from a previous report (Figure 3a,d). In the XPS survey results of the CCS/ZnS QDs prepared in this study (Figure 3d), Cu 2p and Cr 2p peaks were observed in the spectra with the presence of Zn 2p, indicating that the core−shell structure was well prepared via the present synthesis method. It was confirmed that there was no significant difference between the previous and current works on CCS/ZnS QDs. For a more detailed comparison between previous and current studies, HR-XPS analysis was conducted. Interestingly, when we compared the S 2p spectra with previous work (Figure 3b,3e), the intensity of the SO_4^{2-} chemical state at ∼167 eV[29] decreased and the disulfide bonding character[15] disappeared in this work (Figure 3e). These results imply that the impurity may contain sulfate salts, which were removed during the intermediate centrifugation step. The additional TOPO ligand formed a coordination bond with the Cr^{3+} ion, which suppressed the stacking behavior of the S−Cr−S trigonal layers, indicating that the proposed synthetic modification was effective for the synthesis of high-quality QDs. These phenomena can be explained by comparing the Cr 2p XPS profiles (Figure 3c,3f). The peaks of Cr $2p_{3/2}$ and $2p_{1/2}$ were slightly shifted from 576.57 to 575.35 eV, and from 586.25 to 585.35 eV, respectively,[30] with a decrease in the signal intensity. A previous study confirmed Cr_2S_3 NFs as a byproduct during synthesis. To suppress byproduct formation, we employed a co-ligand system by introducing TOPO into the synthetic process. We conclude that this phenomenon can be attributed to TOPO. Cr^{3+} ions may form a relatively robust coordination bond with the P═O dipolar bond of TOPO. TOPO was removed from the system during the purification step, resulting in a Cr 2p chemical shift toward a lower binding energy, probably because of the surface defect sites on the NCs. Moreover, TOPO is a well-known metal cation extraction agent that might decrease Cr^{3+} peak intensity.[26,27] Analysis of other metal precursors (Figure S2) confirmed that the modification did not cause significant side effects on the chemical oxidation states or binding features of the metal cations. The Cu 2p spectra showed no significant difference between previous and present reports, with peaks of Cu $2p_{3/2}$ and $2p_{1/2}$ at ∼932 eV and ∼951.5 eV,[31,32] respectively (Figure S2a,b). This might imply that our modification did not cause any unwanted states such as Cr(II), Cr(VI), and Cu(II) states. The analysis results of ZnS shell-overcoated samples also indicated that the modified method did not affect the process, as witnessed by the peaks of Zn $2p_{3/2}$ and $2p_{1/2}$ at ∼1021 and ∼1044 eV, and S $2p_{3/2}$ and $2p_{1/2}$ at ∼161.5 and ∼163 eV (Figure S2c−f), respectively, with an area ratio of 2.0 implying spin−orbit coupling state.[33]

To characterize the optical properties of the CCS/ZnS QDs, UV−vis and PL spectrometry measurements were conducted (Figure 4). It is worth noting that the $CuInS_2$ core QDs are less- or nonfluorescent.[34] Similar to our previous work, only CCS/ZnS QDs were analyzed by photoluminescence spectrometry for fluorescent property analysis because the CCS-core NCs exhibited a phenomenon analogous to that of the CIS core. However, in the absorption spectra, the specific absorption was blue-shifted from ∼430 nm (CCS core NCs) to ∼380 nm (CCS/ZnS QDs) (Figure 4a). This phenomenon is similar to typical CIS/ZnS QDs formation, indicating a well-

https://doi.org/10.1021/acssuschemeng.3c06115
ACS Sustainable Chem. Eng. 2024, 12, 2588−2597

overcoated ZnS shell on the CCS core NCs. The optical band gaps of the samples were calculated using the Tauc plot equation

$$E = (\alpha h\nu)^{1/2}$$

where E is the optical energy band gap of sample, α is the optical density of sample, h is Planck's constant, and ν is the velocity of light.

The Tauc plot is a powerful method for calculating the optical band gap of material because the entire ensemble of the system determines it. However, some distortion might appear because of absorbing impurities that cause absorption spectra distortion, resulting in some perversion of the result.[35] Nevertheless, the absorption spectra showed a blue shift with an indistinctive entire spectral difference (Figure 4a) and Tauc plot calculation indicated that optical band gaps of CCS NCs and CCS/ZnS QDs are ∼2.56 and 2.75 eV, respectively (inset of Figure 4a). This could also be explained by the ZnS shell overcoating the CCS core NCs. The PL emission properties of the CCS/ZnS QDs were identified as PL maxima at ∼430 nm with a PLE maximum of ∼365 nm (Figure 4b). The Stern−Volmer equation was used to calculate the relative PLQY[18]

$$Q_f = Q_r \frac{I_f A_r n_f^2}{I_r A_f n_r^2}$$

where Q and I are the quantum yield and the integration of the PL emission spectrum, respectively; A is the optical density of the material; and n is the refractive index of the solvent at emission wavelength. Subscripts r and f refer to the reference material and sample, respectively. The calculated PLQY was ∼0.16, indicating that the quality of the CCS/ZnS QDs was improved by this controlled system (Figure 4b). The overall fluorescence was expressed by the PL mapping analysis results, as shown in Figure 4c. Lifetime decay is an important parameter for QDs, and the average fluorescence lifetime of CCS/ZnS QDs prepared in this experiment was confirmed to be 4.08 ns, which is quite different from that of our previous work, probably because of the enhanced passivation of surface defects, resulting in a fast radiative recombination process (Figure 4d). Also, the band structure analysis results of CCS/ZnS QDs revealed that the PL emission mechanism of CCS/ZnS QDs differs from the mechanism of traditional CIS QDs. The redox potentials were calibrated with the below equation

$$E_{LUMO}: -e(E_{red,vsNHE} + 4.71)\ (eV)$$

$$E_{HOMO}: -e(E_{oxi,vsNHE} + 4.71)\ (eV)$$

$$E_{NHE}: E_{Ag/AgCl} + 1.91$$

Typically, the PL mechanism of CIS QDs is the Cu-vacancy-centered relaxation process, which was well characterized by CV analysis (Figure S3a,b). It is well known that Cu vacancy induces a trap state in the QD, resulting in much longer fluorescence lifetime decay.[36−39] However, the case of CCS/ZnS showed no characteristic reduction peak, indicating that the Cu vacancy was not present in the CCS/ZnS QDs (Figure S3c,d). The other orbital states were well matched with UV−vis optical band gap calculation (optical band gap of ∼2.78 eV) and PL emission spectra (PL max at ∼430 nm). This vacancy-free state might cause much faster fluorescence lifetime decay. The photostability of QDs is another important parameter for their utilization in various fields. To evaluate the photostability of CCS/ZnS QDs, the QD solution (10 mg/mL in chloroform) containing a four-plane quartz cuvette was placed in a home-built dark-room chamber, and a 365 nm UV lamp (350 $\mu W/cm^2$) was placed onto the chamber at a distance of 15 cm. The peak intensity of PL spectra of the solution was measured with time intervals. The result showed prominent photostability under 365 nm UV irradiation for several hours under ambient conditions because of the overcoated ZnS shell on the CCS core (Figure 4e). A comparison of the overall optical properties between the previous report and this study is shown in Figure 4f. With synthetic modification, the PL max shifted from ∼465 to 430 nm, closer to the blue spectral region. Furthermore, PLQY was enhanced from ∼0.05 to ∼0.16, which means that the modified CCS/ZnS QD could be a suitable material for blue-emissive probe in optoelectronic applications.

Synthesis of $CuInS_2$/ZnS/ZnS QDs and Fabrication of White-Light-Converting Film. To fabricate a UV light-pumped white-light-converting film, yellow-emitting CIS QDs, another spectral emitter, were prepared and conjugated to the CCS QDs. However, multicomponent emitter systems usually suffer from reabsorption among the fluorophores.[15,16,40,41] To avoid this situation, the CIS QDs were overcoated with a double ZnS shell on their surface to provide yellow-emitting properties and minimize the reabsorption of blue light from the CCS QDs. In addition, to render a high PLQY and shorter wavelength emission, an off-stoichiometric modification for the CIS core synthesis was conducted with an In/Cu molar ratio of 4.0. The successful synthesis of the CIS/ZnS/ZnS QDs was confirmed by TEM analysis (Figure S4a,b). As shown in Figure S4b, the morphology of prepared CIS/ZnS/ZnS QDs were quasi-spherical shape, and the average size of CIS/ZnS/ZnS QDs was revealed to 4.5 ± 1.0 nm, A relatively broad size distribution was confirmed, which might be beneficial for white-light conversion applications, resulting in a broad range emitting phenomenon.[41]

The photoluminescence property of the CIS/ZnS/ZnS QDs was identified to fabricate the white-light-converting layer, and the result is shown in Figure S4c. The PL max of the CIS/ZnS/ZnS QDs was ∼580 nm, with a PLE max at 395 nm. The relative PLQY of the CIS/ZnS/ZnS QDs was also calculated using the Stern−Volmer equation and was confirmed to ∼0.7. For the white-light-converting layer consisting of two fluorophores, blue and yellow, emissive probes are usually employed for two-band spectral white-light emission.[41,42] The CCS/ZnS QDs and CIS/ZnS/ZnS QDs (Figure S4d) were satisfactory for these spectral windows. To fabricate white-light-converting films, it should be noted that the multi-fluorophore system may suffer from light reabsorption, resulting in poor light-converting performance.[15,16,40] To avoid this, the CIS QDs were coated with a double ZnS shell to modify the PLE spectral region, e.g., large Stokes shift.[19] As shown in Figure 4c, the PLE of the CCS/ZnS QDs ranges from 320 to ∼400 nm for blue emission. The PLE range of the CIS/ZnS/ZnS QDs was from 330 to ∼420 nm (Figure S4c), and after that range, the PLQY dramatically decreased. These results imply that the dual ZnS shell may minimize blue light reabsorption and that these two materials can be implemented together in white-light-converting films with high light conversion efficiency and better light temperature controllability.

To fabricate a UV-light-pumped white-light-converting composite, poly(methyl methacrylate) (PMMA) was chosen

https://doi.org/10.1021/acssuschemeng.3c06115
ACS Sustainable Chem. Eng. 2024, 12, 2588−2597

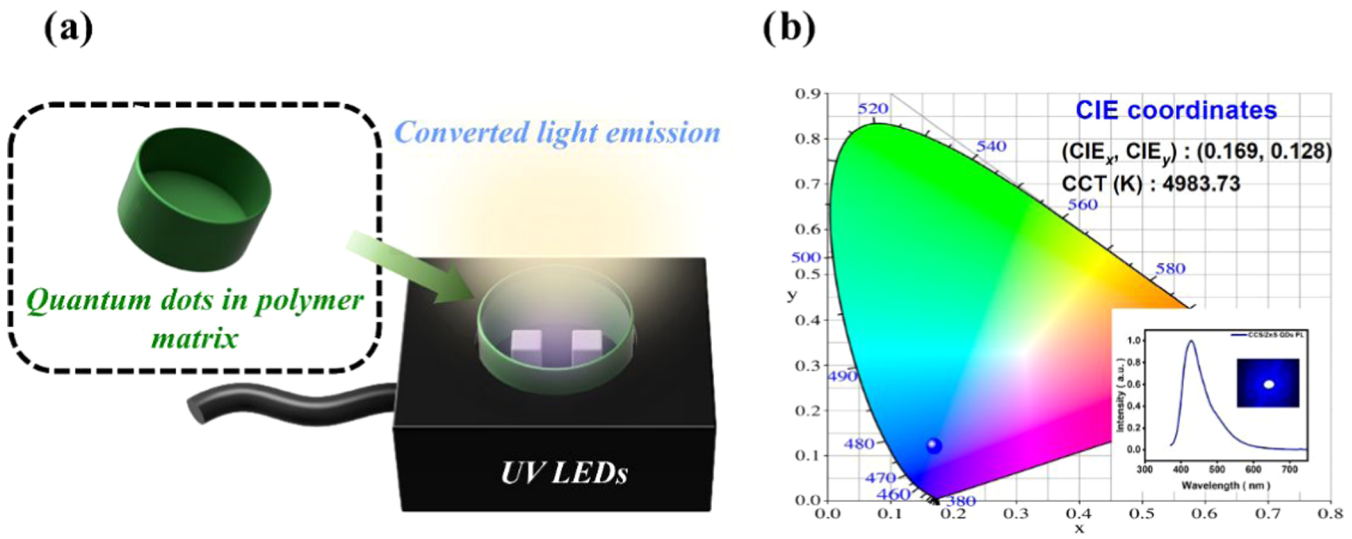

Figure 5. (a) Schematic illustration of a light-converting system with 365 nm UV LEDs; (b) CIE color coordinates and CCT of CCS/ZnS QDs composites with the corresponding PL spectra and LED operation photographs (interpolation).

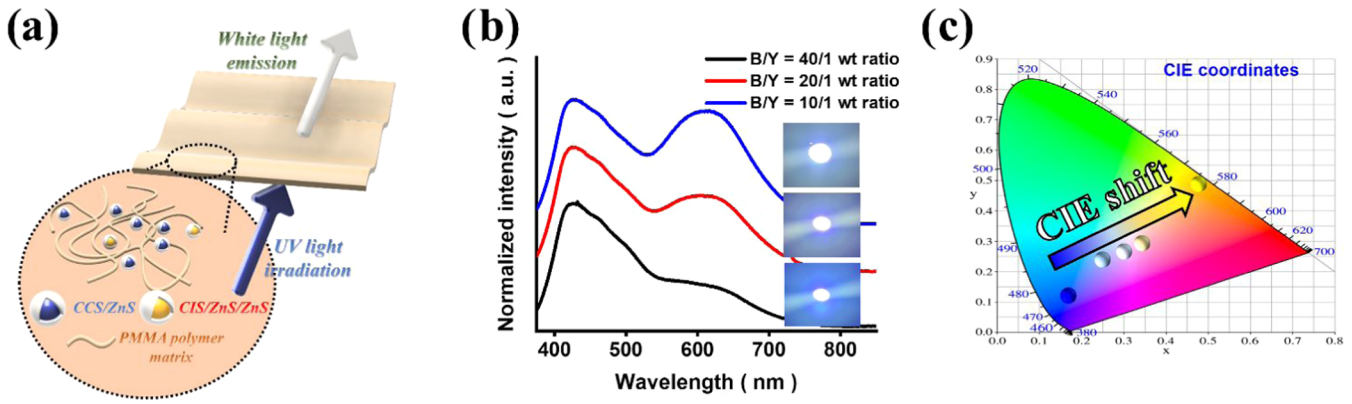

Figure 6. (a) Schematic illustration of white-light-converting systems. (b) PL spectra of B/Y40, B/Y20, and B/Y10 composites and their corresponding LED operation photographs (interpolation). (c) Trend of CIE color coordinates changes with modification of CCS/ZnS QDs and CIS/ZnS/ZnS QDs ratio in the PMMA matrix.

as the supporting matrix of the film. PMMA is a type of thermoplastic polymer with advantages, such as low density and easy processability, which show the properties of the sharp memory effect,[43] resulting in its wide application in many commercial applications.[44] It is well known that PMMA is an optically inactive feature over the 300 nm spectral region, which is beneficial for LED pumped light-converting system.[45,46] The light-converting composite was fabricated using simple drop-casting and drying processes (Figure S5), and the PMMA concentration was fixed at 5 wt % in chloroform.

An overall system description of white LEDs (WLEDs) operation is shown in Figure 5a. We assumed that two independent probes in an optically inactive polymer matrix generate white light under 365 nm UV light irradiation. It is worth noting that the commercially available 365 nm UV-LED system (Prime-100 series, Republic of Korea) with total optical power density of ∼4.5 W was employed, to readily confirm and compare the performance of those composites. Before white LED fabrication, CCS-only and CIS-only composites were fabricated to confirm the light-converting properties of the proposed composites. If the composites can convert UV light to a specific wavelength, the CCS-only and CIS-only composites will display blue and yellow color emission, respectively; the results are shown in Figures 5b and S6. Based on our assumption, these composites clearly exhibited blue and yellow PL spectra with a 365 nm excitation wavelength (interpolated graphs in Figures 5b and S6). Based on these results, the light-conversion performance was confirmed via LED operation (below the interpolated photographs in Figures 5b and S6). The corresponding Commission Internationale de l'Eclairage (CIE) color coordinates indicated that the QDs stably display their intrinsic colors in the PMMA polymer matrix without any interference of matrix matter at a wavelength of 365 nm. As a result, the CIE color coordinates were (CIE$_x$, CIE$_y$ = 0.169, 0.128) for the CCS-only composite and (CIE$_x$, CIE$_y$ = 0.478, 0.498) for the CIS-only composite (Figures 5b and S5).

In white LED applications, CIE color coordinates and CCT are important parameters for the characterization of LEDs or light-converting applications,[47,48] and in our study, we fabricated WLED films by simply mixing the two probes in specific weight ratios. These parameters were controlled by adjusting the ratios between CCS/ZnS QDs and CIS/ZnS/ZnS QDs. The ratios of CCS/ZnS QDs and CIS/ZnS/ZnS QDs were modified to 40.0, 20.0, and 10.0 (w/w); for

https://doi.org/10.1021/acssuschemeng.3c06115
ACS Sustainable Chem. Eng. 2024, 12, 2588−2597

convenience, these composites were denoted as B/Y40, B/Y20, and B/Y10, respectively. The schematic illustration of the light-conversion operation is shown in Figure 6a. The PL spectra of each composite indicated a two-band spectral fluorescence behavior with an excitation wavelength of 365 nm (Figure 6b). With an increase in the number of CIS/ZnS/ZnS QDs, the portion of the yellow spectral region gradually increased without an insignificant effect on the blue spectral window, indicating that blue light reabsorption by CIS/ZnS/ZnS QDs was suppressed, as we assumed (Figure 6b). The corresponding operation photographs are shown in Figure 6b (inset of Figure 6b). These results clearly showed the LED light controllability from bluish-white light to true white light with an increase in the CIS/ZnS/ZnS QDs weight ratio. The trend of the CIE coordinates and CCT transition could be evidence of WLED property control (Figure 6c). The (CIE_x, CIE_y) coordinates and CCT were effectively moved from (0.254, 0.245, and 21914.48 K) (B/Y40) to (0.302, 0.278, and 8217.77 K) (B/Y20), and eventually (0.34, 0.299, and 5071.39 K) (B/Y10), implying successful modification of the WLED properties. Additionally, we investigated the photo- and thermal stabilities of the WLED film (Figure S7). Our system showed prominent photostability with mere CIE color shifting for 12 h under UV-LED light at room temperature. Also, the CIE color coordinates were steady under UV-LED light at 80 °C for 4 h, showing enough thermal stability.

CONCLUSIONS

In our previous work, we synthesized CCS/ZnS QDs. Poor quality of the synthesized QDs was observed owing to the unbalanced metal cation reactivities toward the sulfur source (thiol), resulting in the formation of ternary composite QDs and separate metal sulfide Cr_2S_3 NFs. In this study, the successful synthesis of $CuCrS_2$/ZnS (CCS/ZnS) QDs as blue-emitting probes was confirmed via metal precursor modification and a co-ligand system. To enhance the quality of the QDs, the reactivity of the monovalent cation, Cu^+, was suppressed because the reactivity of Cu^+-thiol is much higher than that of Cr^{3+}-thiol, according to hard and soft acids and bases (HSAB) theory. In addition, trioctylphosphine oxide (TOPO), a highly polarizable ligand molecule, was incorporated into the system to suppress side-product formation, Cr_2S_3 NFs, via strong binding affinity toward Cr^{3+} and the steric hindrance effect. The resulting CCS/ZnS QDs showed improved morphological features, for example, uniform morphology and narrow size distribution, with an average diameter of 5.5 ± 0.6 nm. The CCS/ZnS QDs exhibited blue-shifted absorption spectra compared to the uncoated CCS NCs. The introduction of the ZnS shell overcoating onto the CCS NCs resulted in fluorescence properties with PLE max ~430 nm under PLE max ~365 nm (PLQY ~ 0.16), owing to the passivation of surface defects, enhancing the radiative recombination of excitons. To confirm the possibility of their application in the optoelectronic field, CCS/ZnS QDs were incorporated with yellow-emitting CIS/ZnS/ZnS QDs in a PMMA polymer matrix and the fabricated composite was employed for white-light conversion under UV light (365 nm) irradiation. The resulting properties were (CIE_x, CIE_y = 0.254, 0.245) and T_c ~ 21914.48 K, respectively, indicating cold-temperature white-light emission. Color coordinates and T_c parameters were successfully modified to (CIE_x, CIE_y = 0.34, 0.299) and T_c ~ 5071.49 K by the ratio control of CCS/ZnS QDs and CIS/ZnS/ZnS QDs (from 40.0 to 10.0, w/w). Thus, these QDs have great potential to be building blocks for optoelectronics away from environmental regulation.

ASSOCIATED CONTENT

Supporting Information

The Supporting Information is available free of charge at https://pubs.acs.org/doi/10.1021/acssuschemeng.3c06115.

Comparison among $CuCrS_2$-related seminal research articles, and our works (Table S1); elemental ratio analysis and comparison results of prepared QDs (Table S2); XRD analysis results of $CuCrS_2$ core and $CuCrS_2$/ZnS QDs (Figure S1); Cu 2p, Zn 2p, and S 2p XPS analysis results (Figure S2); CV analysis results of $CuInS_2$/ZnS/ZnS QDs and $CuCrS_2$/ZnS QDs (Figure S3); morphological and optical analysis of $CuInS_2$/ZnS/ZnS QDs (Figure S4); schematic illustration of light-converting film fabrication (Figure S5); and light-converting property analysis of $CuInS_2$/ZnS/ZnS QDs-only composite (Figure S6), photo- and thermal stability test results of WLED film (Figure S7) (PDF)

AUTHOR INFORMATION

Corresponding Author

Chan Ho Park − *Department of Chemical and Biological Engineering, Gachon University, Seongnam 13120, Republic of Korea;* orcid.org/0000-0002-1832-4842; Email: chhopark@gachon.ac.kr

Authors

Ho Kyung Lee − *Department of Chemical and Biological Engineering, Gachon University, Seongnam 13120, Republic of Korea; Smart Materials Research Center for IoT, Gachon University, Seongnam 13120, Republic of Korea*

Ji Hyeon Kim − *Department of Chemical and Biological Engineering, Gachon University, Seongnam 13120, Republic of Korea*

Il Tae Kim − *Department of Chemical and Biological Engineering, Gachon University, Seongnam 13120, Republic of Korea;* orcid.org/0000-0002-8857-0061

Dal Ho Lee − *Department of Electronic Engineering, Gachon University, Seongnam 13120, Republic of Korea*

Complete contact information is available at: https://pubs.acs.org/10.1021/acssuschemeng.3c06115

Notes

The authors declare no competing financial interest.

ACKNOWLEDGMENTS

This research was supported by the Basic Science Research Capacity Enhancement Project through the Korea Basic Science Institute (National Research Facilities and Equipment Center) grant funded by the Ministry of Education (2019R1A6C1010016) and the National Research Foundation of Korea (NRF) grant funded by the Korea government (MSIT) (RS-2023−00251670).

REFERENCES

(1) Murray, C. B.; Norris, D. J.; Bawendi, M. G. Synthesis and characterization of nearly monodisperse CdE (E= sulfur, selenium, tellurium) semiconductor nanocrystallites. *J. Am. Chem. Soc.* **1993**, *115* (19), 8706−8715.

(2) Dabbousi, B. O.; Rodriguez-Viejo, J.; Mikulec, F. V.; Heine, J. R.; Mattoussi, H.; Ober, R.; Jensen, K. F.; Bawendi, M. G. (CdSe) ZnS core− shell quantum dots: synthesis and characterization of a size series of highly luminescent nanocrystallites. *J. Phys. Chem. B* **1997**, *101* (46), 9463−9475.
(3) Foda, M. F.; Huang, L.; Shao, F.; Han, H. Y. Biocompatible and highly luminescent near-infrared $CuInS_2$/ZnS quantum dots embedded silica beads for cancer cell imaging. *ACS Appl. Mater. Interfaces* **2014**, *6* (3), 2011−2017.
(4) Zhao, C.; Bai, Z.; Liu, X.; Zhang, Y.; Zou, B.; Zhong, H. Small GSH-Capped $CuInS_2$ Quantum Dots: MPA-Assisted Aqueous Phase Transfer and Bioimaging Applications. *ACS Appl. Mater. Interfaces* **2015**, *7* (32), 17623−17629.
(5) Arshad, A.; Akram, R.; Iqbal, S.; Batool, F.; Iqbal, B.; Khalid, B.; Khan, A. U. Aqueous synthesis of tunable fluorescent, semiconductor $CuInS_2$ quantum dots for bioimaging. *Arabian J. Chem.* **2019**, *12* (8), 4840−4847.
(6) Safari, S.; Amiri, A.; Badiei, A. Selective detection of aspartic acid in human serum by a fluorescent probe based on $CuInS_2$@ZnS quantum dots. *Spectrochim. Acta, Part A* **2023**, *291*, No. 122294.
(7) Speranskaya, E. S.; Beloglazova, N. V.; Abe, S.; Aubert, T.; Smet, P. F.; Poelman, D.; Goryacheva, I. Y.; De Saeger, S.; Hens, Z. Hydrophilic, bright $CuInS_2$ quantum dots as Cd-free fluorescent labels in quantitative immunoassay. *Langmuir* **2014**, *30* (25), 7567−7575.
(8) Neo, D. C. J.; Goh, W. P.; Lau, H. H.; Shanmugam, J.; Chen, Y. F. $CuInS_2$ Quantum Dots with Thick ZnSexS1−x Shells for a Luminescent Solar Concentrator. *ACS Appl. Nano Mater.* **2020**, *3* (7), 6489−6496.
(9) Kim, S.; Kim, J.-A.; Kim, T.; Chung, H.; Park, S.; Choi, S.-M.; Kim, H.-M.; Chung, D.-Y.; Jang, E. Efficient Blue-Light-Emitting Cd-Free Colloidal Quantum Well and Its Application in Electroluminescent Devices. *Chem. Mater.* **2020**, *32* (12), 5200−5207.
(10) Lim, J.; Park, M.; Bae, W. K.; Lee, D.; Lee, S.; Lee, C.; Char, K. Highly efficient cadmium-free quantum dot light-emitting diodes enabled by the direct formation of excitons within InP@ ZnSeS quantum dots. *ACS Nano* **2013**, *7* (10), 9019−9026.
(11) Eren, G. O.; Sadeghi, S.; Jalali, H. B.; Ritter, M.; Han, M.; Baylam, I.; Melikov, R.; Onal, A.; Oz, F.; Sahin, M.; Ow-Yang, C. W.; Sennaroglu, A.; Lechner, R. T.; Nizamoglu, S. Cadmium-Free and Efficient Type-II InP/ZnO/ZnS Quantum Dots and Their Application for LEDs. *ACS Appl. Mater. Interfaces* **2021**, *13* (27), 32022−32030, DOI: 10.1021/acsami.1c08118.
(12) Jang, H. S.; Won, Y. H.; Jeon, D. Y. Improvement of electroluminescent property of blue LED coated with highly luminescent yellow-emitting phosphors. *Appl. Phys. B* **2009**, *95* (4), 715−720, DOI: 10.1007/s00340-009-3484-1.
(13) Jang, H. S.; Kwon, B.-H.; Yang, H.; Jeon, D. Y. Bright three-band white light generated from CdSe/ZnSe quantum dot-assisted Sr_3SiO_5:Ce^{3+},Li^+-based white light-emitting diode with high color rendering index. *Appl. Phys. Lett.* **2009**, *95* (16), No. 161901, DOI: 10.1063/1.3246800.
(14) Jang, H. S.; Yang, H.; Kim, S. W.; Han, J. Y.; Lee, S. G.; Jeon, D. Y. White Light-Emitting Diodes with Excellent Color Rendering Based on Organically Capped CdSe Quantum Dots and Sr_3SiO_5:Ce^{3+}, Li^+ Phosphors. *Adv. Mater.* **2008**, *20* (14), 2696−2702.
(15) Won, Y.-H.; Jang, H. S.; Im, W. B.; Jeon, D. Y.; Lee, J. S. Tunable full-color-emitting La0. 827Al11. 9O19. 09: Eu^{2+}, Mn^{2+} phosphor for application to warm white-light-emitting diodes. *Appl. Phys. Lett.* **2006**, *89* (23), No. 231909, DOI: 10.1063/1.2398887.
(16) Kim, J. S.; Jeon, P.; Choi, J.; Park, H.; Mho, S.; Kim, G. Warm-white-light emitting diode utilizing a single-phase full-color $Ba_3MgSi_2O_8$: Eu^{2+}, Mn^{2+} phosphor. *Appl. Phys. Lett.* **2004**, *84* (15), 2931−2933.
(17) Levina, A.; Lay, P. A. Chemical properties and toxicity of chromium (III) nutritional supplements. *Chem. Res. Toxicol.* **2008**, *21* (3), 563−571.
(18) Lee, H. K.; Ban, Y. J.; Lee, H. J.; Kim, J. H.; Park, S. J. One-Pot Synthesis and Characterization of $CuCrS_2$/ZnS Core/Shell Quantum Dots as New Blue-Emitting Sources. *Materials* **2023**, *16* (2), No. 762, DOI: 10.3390/ma16020762.
(19) Leach, A. D. P.; Macdonald, J. E. Optoelectronic Properties of $CuInS_2$ Nanocrystals and Their Origin. *J. Phys. Chem. Lett.* **2016**, *7* (3), 572−583.
(20) Alfarra, A.; Frackowiak, E.; Béguin, F. The HSAB concept as a means to interpret the adsorption of metal ions onto activated carbons. *Appl. Surf. Sci.* **2004**, *228* (1−4), 84−92.
(21) Cammack, R.; Hughes, M. N. In *Considerations for the Specification of Enzyme Assays Involving Metal Ions*, Proceedings of the 3rd Beilstein ESCEC Symposium "Experimental Standard Conditions Of Enzyme Characterization; ESEC, 2008.
(22) Tappan, B. A.; Crans, K. D.; Brutchey, R. L. Formation Pathway of Wurtzite-like $Cu_2ZnSnSe_4$ Nanocrystals. *Inorg. Chem.* **2021**, *60* (22), 17178−17185.
(23) Fan, Y. Z.; Han, L.; Liu, S. G.; Zhang, Y.; Luo, H. Q.; Li, N. B. A ratiometric optical strategy for bromide and iodide ion sensing based on target-induced competitive coordination of a metal−organic nanosystem. *J. Mater. Chem. C* **2020**, *8* (33), 11517−11524.
(24) Fujioka, E.; Nishihara, H.; Aramaki, K. The inhibition of passive film breakdown on iron in a borate buffer solution containing chloride ions by mixtures of hard and soft base inhibitors. *Corros. Sci.* **1996**, *38* (10), 1669−1679.
(25) Liu, F.; Zhang, Y.; Ding, C.; Kawabata, K.; Yoshihara, Y.; Toyoda, T.; Hayase, S.; Minemoto, T.; Wang, R.; Shen, Q. Trioctylphosphine Oxide Acts as Alkahest for SnX_2/PbX_2: A General Synthetic Route to Perovskite $ASn_xPb_{1-x}X_3$ (A = Cs, FA, MA; X = Cl, Br, I) Quantum Dots. *Chem. Mater.* **2020**, *32* (3), 1089−1100.
(26) Mann, C. K.; White, J. C. Extraction of Chromium with Trioctylphosphine Oxide from Acidic Solutions of Alkali Metal Salts. *Anal. Chem.* **1958**, *30* (5), 989−992.
(27) Wardell, J. M.; King, C. J. Solvent equilibriums for extraction of carboxylic acids from water. *J. Chem. Eng. Data* **1978**, *23* (2), 144−148.
(28) Xie, B. B.; Hu, B. B.; Jiang, L. F.; Li, G.; Du, Z. L. The phase transformation of $CuInS_2$ from chalcopyrite to wurtzite. *Nanoscale Res. Lett.* **2015**, *10*, No. 86, DOI: 10.1186/s11671-015-0800-z.
(29) Xueyang, L.; Rutie, L.; Lin, W.; Zhengzhou, L.; Xiang, X.; Ning, L.; Jie, C. The synergistic effect of carbon materials on properties of copper-based friction materials. *Ind. Lubr. Tribol.* **2021**, *73* (1), 170−176.
(30) Chen, Y.; An, D.; Sun, S.; Gao, J.; Qian, L. Reduction and Removal of Chromium VI in Water by Powdered Activated Carbon. *Materials* **2018**, *11* (2), No. 269, DOI: 10.3390/ma11020269.
(31) Tang, Z.; Yeo, B. C.; Han, S. S.; Lee, T. J.; Bhang, S. H.; Kim, W. S.; Yu, T. Facile aqueous-phase synthesis of Ag-Cu-Pt-Pd quadrometallic nanoparticles. *Nano Convergence* **2019**, *6* (1), No. 38, DOI: 10.1186/s40580-019-0208-z.
(32) Kumar, M.; Bhatt, V.; Nayal, O. S.; Sharma, S.; Kumar, V.; Thakur, M. S.; Kumar, N.; Bal, R.; Singh, B.; Sharma, U. CuI nanoparticles as recyclable heterogeneous catalysts for C−N bond formation reactions. *Catal. Sci. Technol.* **2017**, *7* (13), 2857−2864.
(33) Turo, M. J.; Macdonald, J. E. Crystal-Bound vs Surface-Bound Thiols on Nanocrystals. *ACS Nano* **2014**, *8* (10), 10205−10213.
(34) van der Stam, W.; de Graaf, M.; Gudjonsdottir, S.; Geuchies, J. J.; Dijkema, J. J.; Kirkwood, N.; Evers, W. H.; Longo, A.; Houtepen, A. J. Tuning and Probing the Distribution of Cu^+ and Cu^{2+} Trap States Responsible for Broad-Band Photoluminescence in $CuInS_2$ Nanocrystals. *ACS Nano* **2018**, *12* (11), 11244−11253.
(35) de Mello Donegá, C.; Koole, R. Size Dependence of the Spontaneous Emission Rate and Absorption Cross Section of CdSe and CdTe Quantum Dots. *J. Phys. Chem. C* **2009**, *113* (16), 6511−6520.
(36) Knowles, K. E.; Nelson, H. D.; Kilburn, T. B.; Gamelin, D. R. Singlet-Triplet Splittings in the Luminescent Excited States of Colloidal Cu^+:CdSe, Cu^+:InP, and CuInS2 Nanocrystals: Charge-Transfer Configurations and Self-Trapped Excitons. *J. Am. Chem. Soc.* **2015**, *137* (40), 13138−13147.

(37) Binsma, J.; Giling, L.; Bloem, J. Luminescence of $CuInS_2$: I. The broad band emission and its dependence on the defect chemistry. *J. Lumin.* **1982**, *27* (1), 35−53.
(38) Binsma, J.; Giling, L.; Bloem, J. Luminescence of $CuInS_2$: II. Exciton and near edge emission. *J. Lumin.* **1982**, *27* (1), 55−72.
(39) Fuhr, A. S.; Yun, H. J.; Makarov, N. S.; Li, H.; McDaniel, H.; Klimov, V. I. Light Emission Mechanisms in $CuInS_2$ Quantum Dots Evaluated by Spectral Electrochemistry. *ACS Photonics* **2017**, *4* (10), 2425−2435.
(40) Kim, J. S.; Jeon, P. E.; Park, Y. H.; Choi, J. C.; Park, H. L.; Kim, G. C.; Kim, T. W. White-light generation through ultraviolet-emitting diode and white-emitting phosphor. *Appl. Phys. Lett.* **2004**, *85* (17), 3696−3698.
(41) Park, S. H.; Hong, A.; Kim, J. H.; Yang, H.; Lee, K.; Jang, H. S. Highly bright yellow-green-emitting $CuInS_2$ colloidal quantum dots with core/shell/shell architecture for white light-emitting diodes. *ACS Appl. Mater. Interfaces* **2015**, *7* (12), 6764−6771.
(42) Sadeghi, S.; Abkenar, S. K.; Ow-Yang, C. W.; Nizamoglu, S. Efficient White LEDs Using Liquid-state Magic-sized CdSe Quantum Dots. *Sci. Rep.* **2019**, *9* (1), No. 10061, DOI: 10.1038/s41598-019-46581-2.
(43) Xi, F.; Bartus, J.; Vogl, O. Optical activity measurements on solids. 3. Non-optically active synthetic polymers. *Polym. Int.* **1993**, *31* (2), 183−196.
(44) Samal, S.; Kosjakova, O. Surface feature of PMMA films on NiTi alloy substrate by the spin coating method. *Ceram. Int.* **2023**, *49* (14), 24370−24378.
(45) Rezig, H.; Vitrant, G. Feasibility of optically controlled integrated Mach−Zehnder device based on Azo dye-doped PMMA thin films. *Opt. Commun.* **2001**, *200* (1), 261−269.
(46) Lanty, G.; Bréhier, A.; Parashkov, R.; Lauret, J. S.; Deleporte, E. Strong exciton−photon coupling at room temperature in micro-cavities containing two-dimensional layered perovskite compounds. *New J. Phys.* **2008**, *10* (6), No. 065007, DOI: 10.1088/1367-2630/10/6/065007.
(47) Tatu, C. Correlated color temperature determination for led modulesusing a digital color sensor. *UPB Sci. Bull. Ser. A Appl. Math. Phys.* **2013**, *75*, 225−232.
(48) Fontecha, J.; Campos, J.; Corróns, A.; Pons, A. An analytical method for estimating correlated colour temperature uncertainty. *Metrologia* **2002**, *39* (6), No. 531, DOI: 10.1088/0026-1394/39/6/3.

https://doi.org/10.1021/acssuschemeng.3c06115
ACS Sustainable Chem. Eng. 2024, 12, 2588−2597